Supplementary Figures and Captions

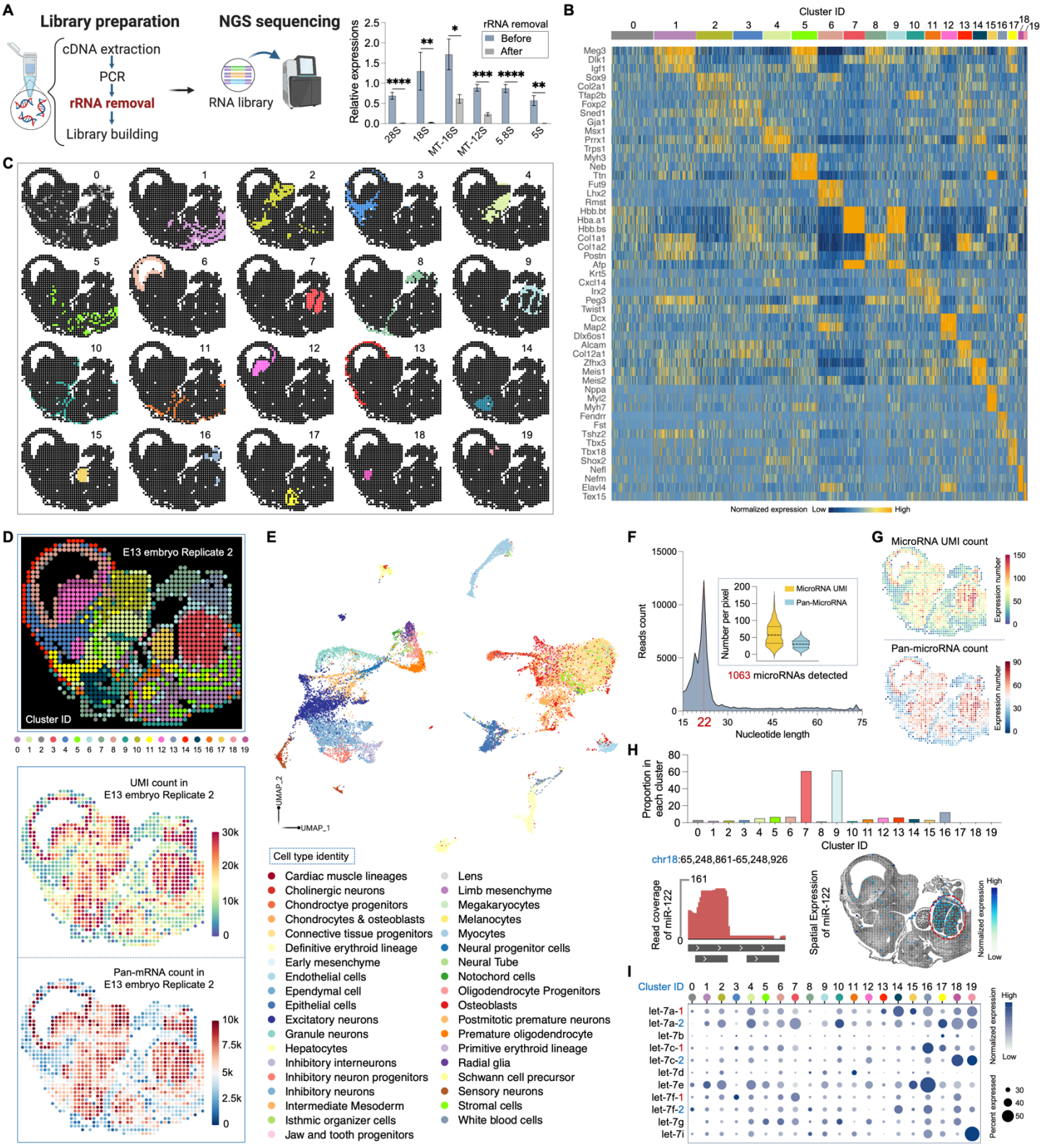

Figure S1. Patho-DBiT performance and spatial microRNA co-profiling in E13 mouse embryo

(**A**) Left: Patho-DBiT steps post tissue barcoding. Right: qPCR analysis of the rRNA removal efficiency.
(**B**) Heatmap showing top ranked differentially expressed genes (DEGs) defining each cluster.
(**C**) Spatial distribution of identified clusters.
(**D**) Top: unsupervised clustering of the replicate E13 mouse embryo section. Bottom: spatial pan-mRNA and UMI count maps of the replicate section.
(**E**) Cell types identified by integrated clustering analysis of combined scRNA-seq reference dataset (Cao et al., *Nature* 2019) and Patho-DBiT data in E13 mouse embryo.
(**F**) Patho-DBiT demonstrates co-profiling of microRNAs in the E13 mouse embryo. The count of mapped microRNA reads peaks at 22 nucleotides in the dataset.
(**G**) Spatial pan-microRNA and corresponding UMI count maps.
(**H**) Top: expression proportion of the liver-specific miR-122 in each identified cluster. Bottom left: read coverage of miR-122 mapped to the reference genome location. Bottom right: spatial distribution of miR-122.
(**I**) The expression landscape of let-7 family of microRNAs in different spatial clusters. Dot size corresponds to the percentage of pixels expressing the gene, while color shade represents expression level.

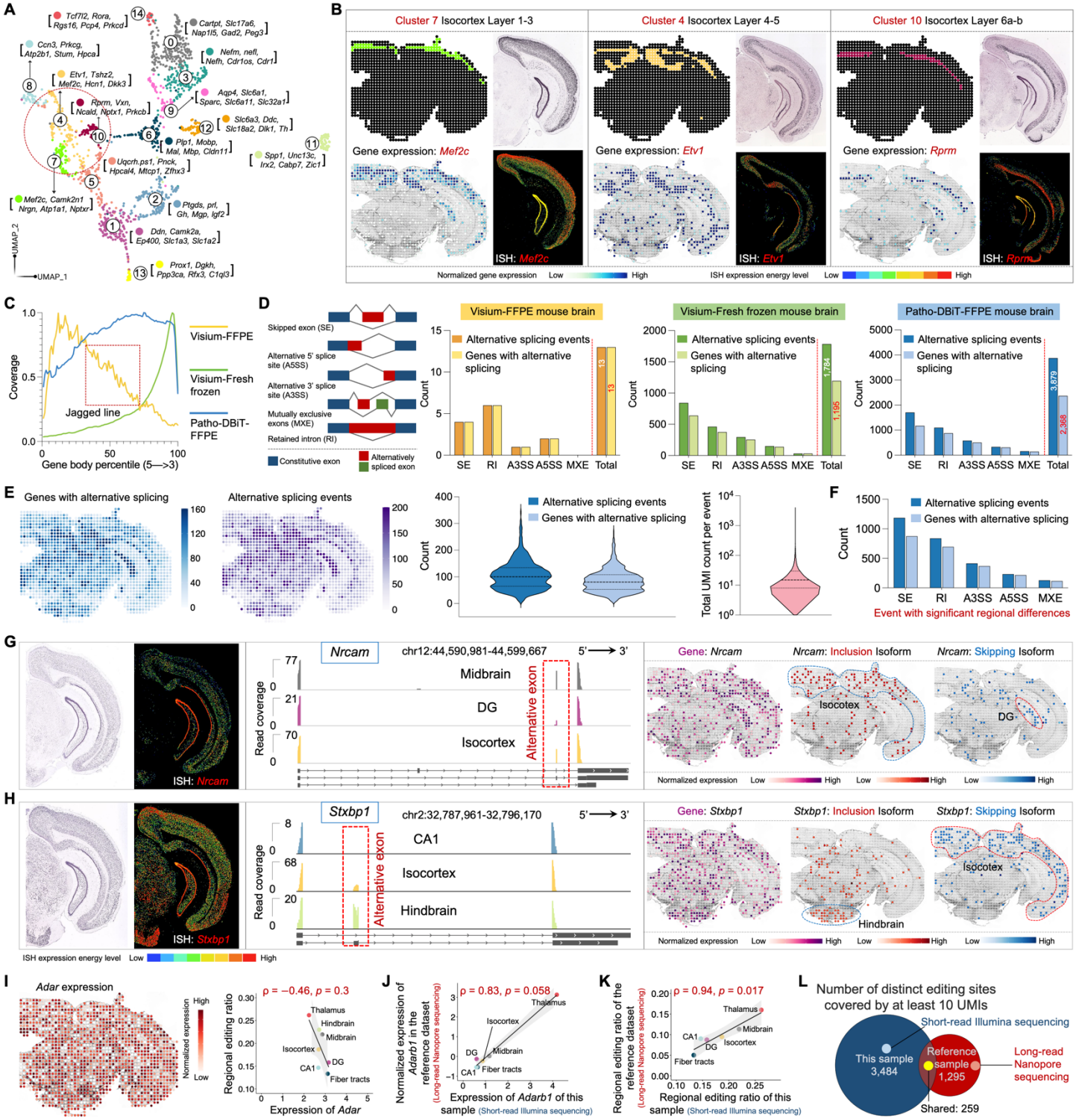

Figure S2. Spatial co-profiling of gene expression, alternative splicing, and A-to-I RNA editing in the mouse brain

(**A**) UMAP showing the clustering analysis of Patho-DBiT data in FFPE mouse brain section. Top 5 genes defining each cluster are indicated.

(**B**) Spatial distribution of clusters 4, 7, 10 in the isocortex region alongside their principle defining genes. ISH staining and expression images are from the Allen Mouse Brain Atlas.
(**C**) Read coverage along the gene body from 5' to 3'. Comparison involves Patho-DBiT data and Visium datasets from 10x Genomics on both FFPE and fresh frozen brain sections.
(**D**) Number of detected spliced events and corresponding parental genes within the three datasets listed in (C).
(**E**) Spatial distribution of the detected spliced events and corresponding parental genes of Patho-DBiT data, along with the UMI count distribution per each splicing event.
(**F**) Number of each event type with significant regional differences.
(**G** and **H**) Junction read coverage of *Nrcam* (G) and *Stxbp1* (H) splicing event in specific brain regions. Spatial expression patterns of the gene, exon inclusion isoform, and exon skipping isoform are shown. ISH staining and expression images are from the Allen Mouse Brain Atlas.
(**I**) Left: spatial *Adar* expression. Right: correlation between the *Adar* expression and the average reginal editing ratio across various brain regions.
(**J** and **K**) Correlation between regional *Adarb1* expression (J) or editing ratio (K) detected by short-read Illumina sequencing-based Patho-DBiT and those detected by long-read Nanopore sequencing (Lebrigand et al., *Nucleic Acids Research* 2023). Note, the hindbrain was not included in the brain sample profiled in the reference dataset.
(**L**) Venn plot showing the count of distinct editing sites covered by a minimum of 10 UMIs in both datasets.

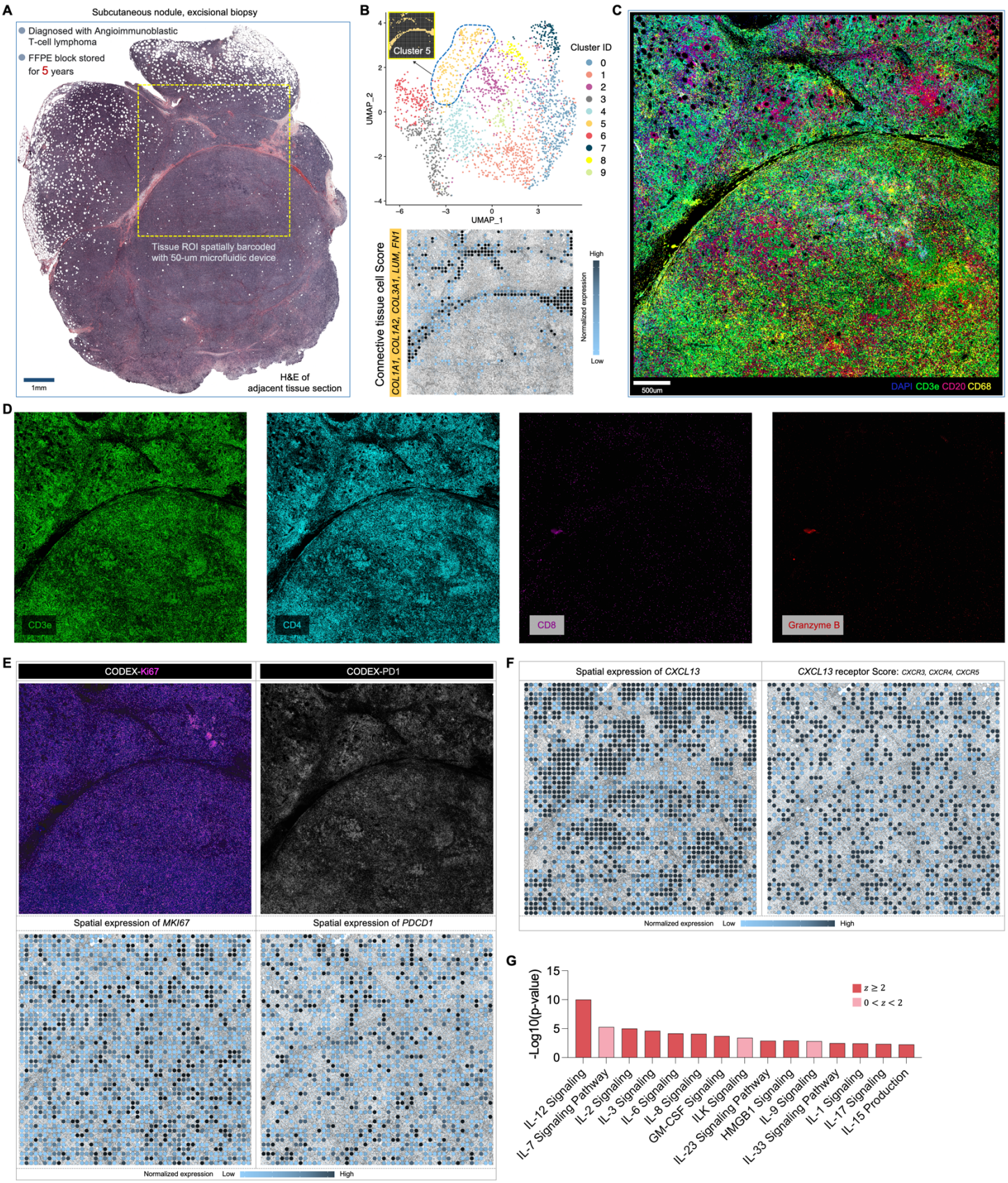

Figure S3. Detection accuracy of Patho-DBiT in the AITL section cross-validated with CODEX

(**A**) Full scan of the H&E staining of an adjacent section. Yellow square indicates the region of interest (ROI) spatially barcoded with the 50 μm-microfluidic device.
(**B**) Top: UMAP showing the clustering analysis of Patho-DBiT data in the AITL section. The spatial distribution of cluster 5 is indicated. Bottom: spatial expression of the Connective tissue cell Score. Genes defining this module score are listed.
(**C**) Enlarged CODEX image corresponding to the ROI barcoded by Patho-DBiT.
(**D**) CODEX images showing expression of CD3e, CD4, CD8, and Granzyme B.
(**E**) Spatial expressions of *MKI67* and *PDCD1* and the corresponding CODEX images of Ki67 and PD-1.
(**F**) Spatial expressions of *CXCL13* and the *CXCL13* receptor Score. Genes defining this module score are listed.
(**G**) Signaling pathways related to T cell functions in Cluster 0. z score is computed and used to reflect the predicted activation level (z>0, activated; z<0, inhibited; z≥2 or z≤−2 can be considered significant).

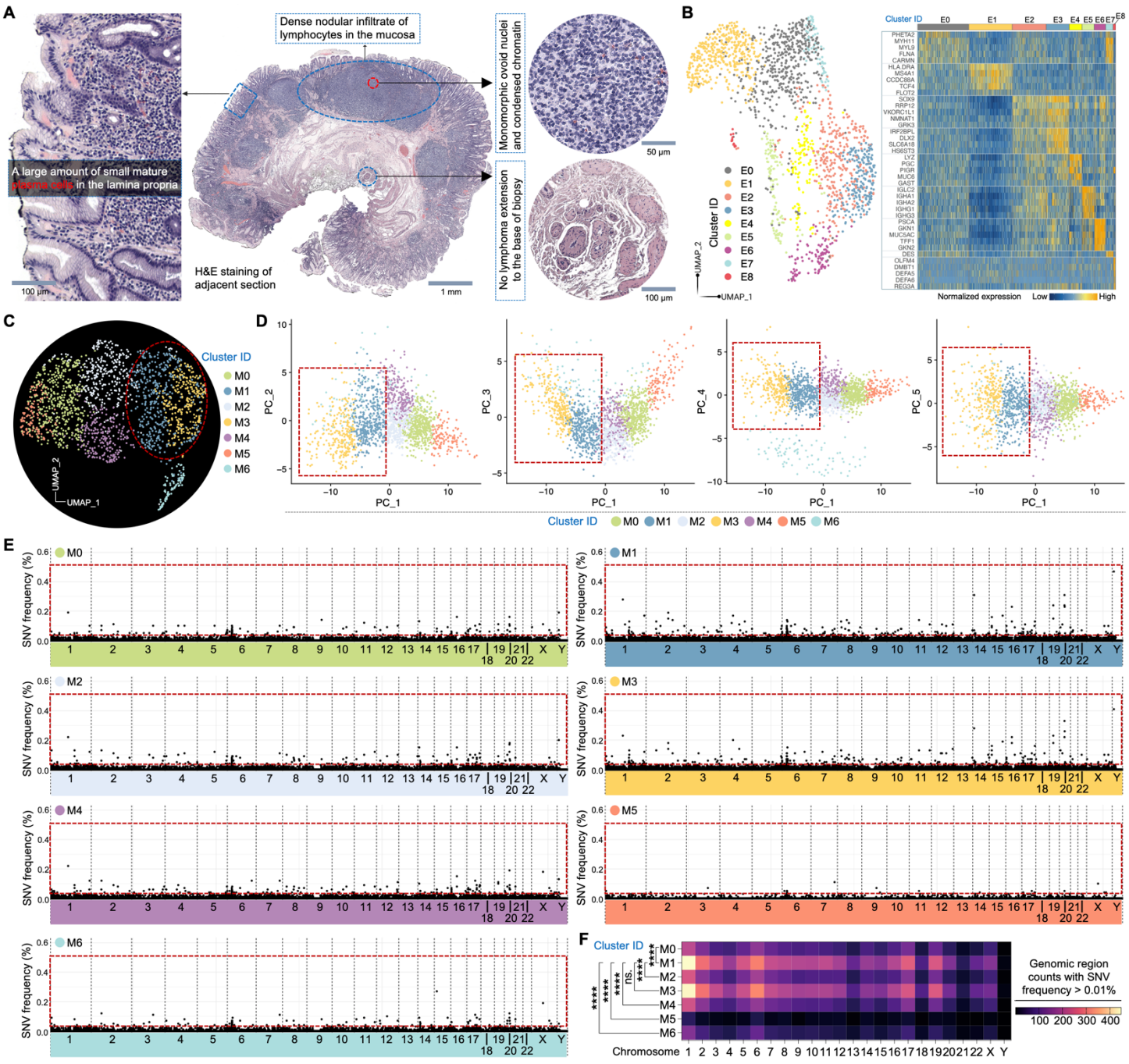

Figure S4. Spatial transcriptome and variation co-profiling of the MALT section

(**A**) H&E staining of an adjacent section with key histological information annotated by a pathologist.
(**B**) Left: UMAP showing the clustering analysis of Patho-DBiT data in the MALT section. Right: heatmap showing top ranked DEGs defining each cluster.
(**C**) UMAP showing the clustering analysis of spatial SNV matrix.
(**D**) Principal component analysis (PCA) of the identified variation clusters in (B). Top5 PCA components were analyzed.

(**E**) Genome-wide distribution of SNV frequency in each variation cluster. The SNV frequency was counted within sliding genomic regions of 10,000 bp.
(**F**) Count comparison of genomic regions with SNV frequency >0.01% between variation clusters.

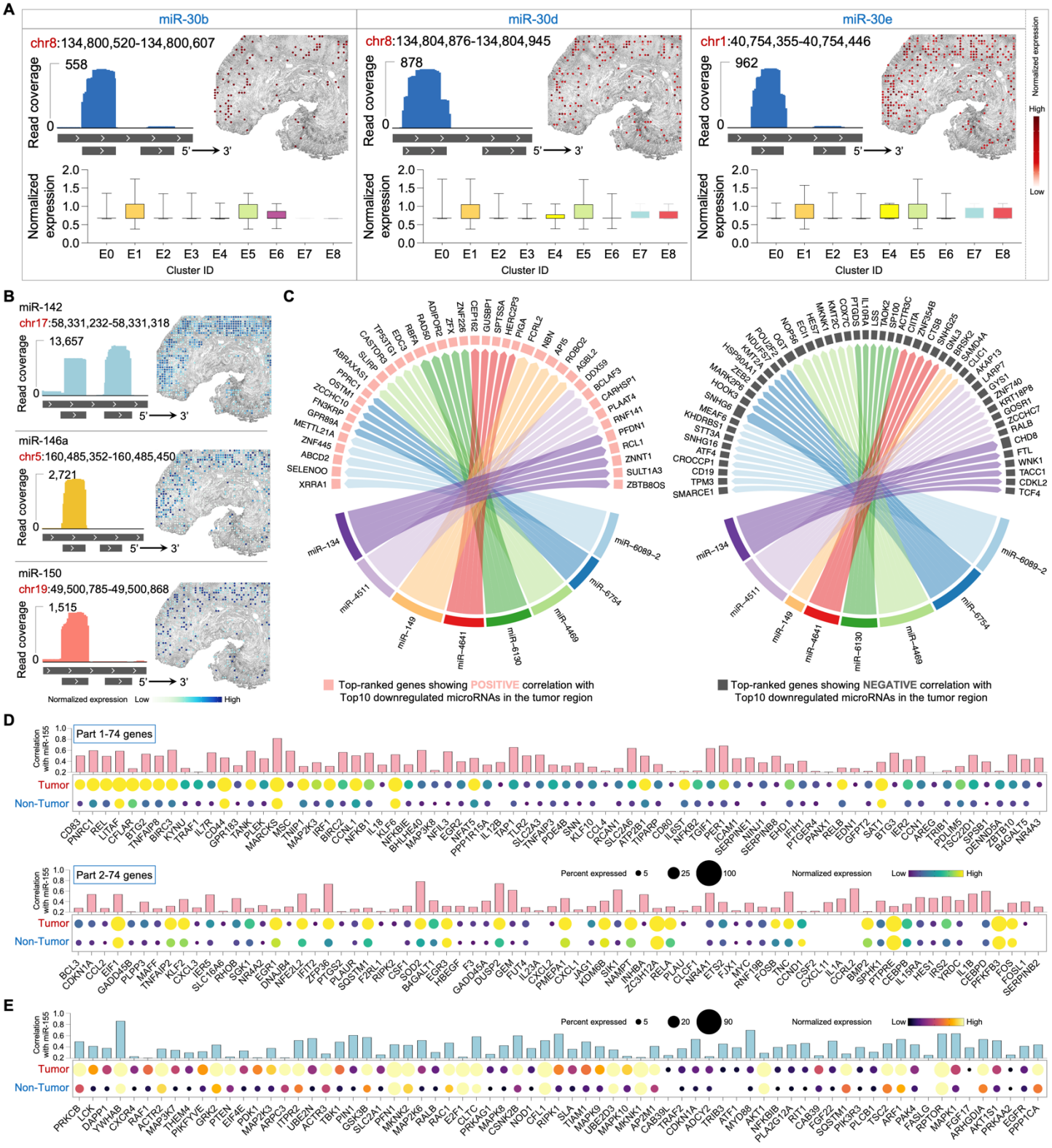

Figure S5. Spatial microRNA profile of the MALT section

(**A**) Spatial mapping of microRNAs in mature B-cell differentiation regulation. The read coverage mapped to the

reference genome location, expression proportion in each identified cluster, and spatial distribution are shown.
(**B**) Spatial mapping of microRNAs enriched in marginal zone B cells or lymphoma. The read coverage mapped to the reference genome location and spatial distribution are shown.
(**C**) Regulatory network between the top 10 downregulated microRNAs and the gene expression in the tumor region. Genes with the highest rankings, demonstrating positive or negative correlations with the microRNAs, were separately illustrated. Edge thickness is proportional to correlation weights.
(**D** and **E**) Correlation analysis between miR-155 and each gene in the GSEA-defined NF-κB signaling (D) or PI3K-AKT signaling (E). Enhanced expression of genes participating in both signaling pathways is observed in the tumor region compared to the non-tumor region. The dot size indicates the percentage of pixels expressing the gene, and the color shade represents normalized expression level.

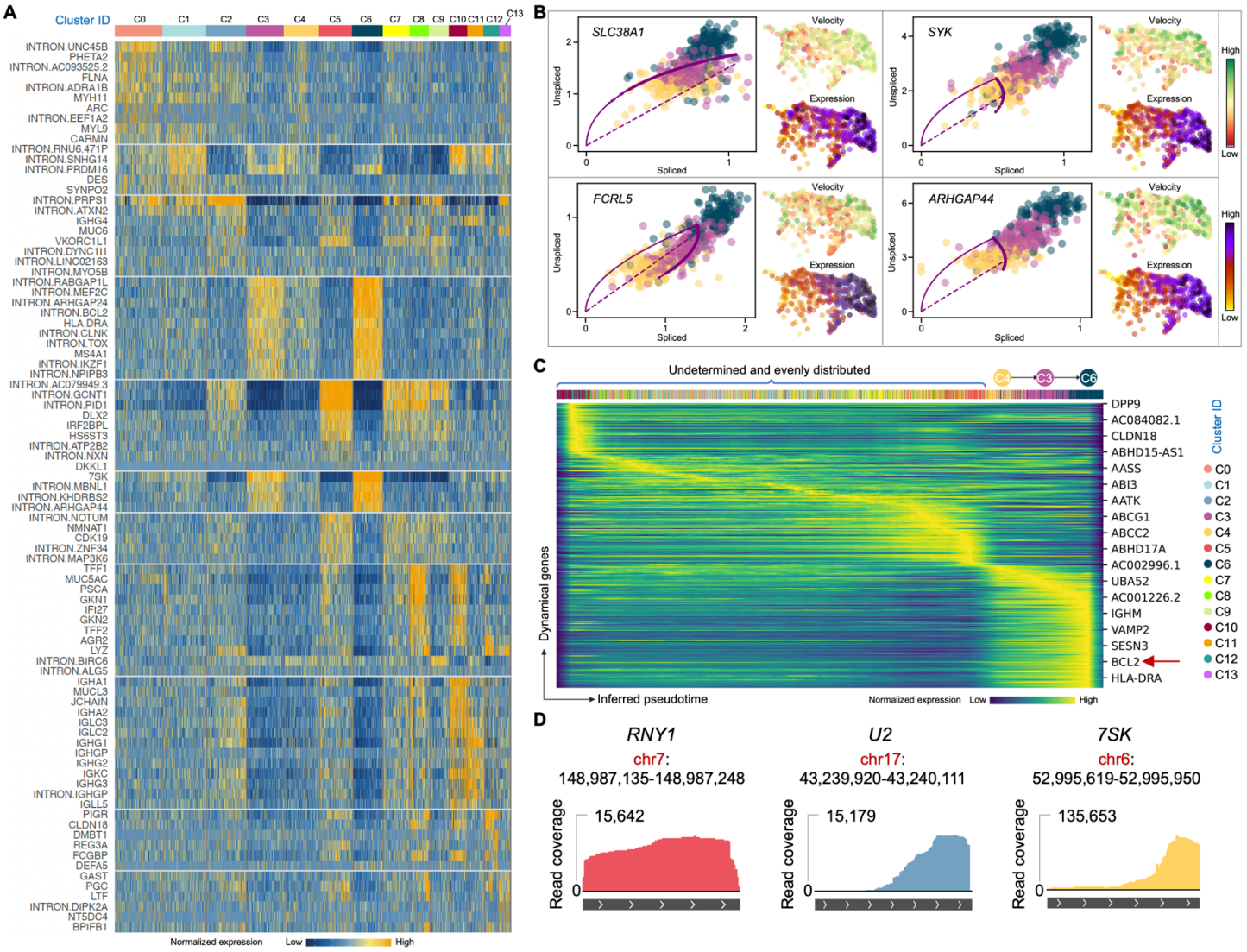

Figure S6. Spatial RNA splicing and pseudotime analysis of the MALT section

(**A**) Heatmap showing top ranked DEGs defining each cluster identified by clustering analysis of the combined exonic and intronic expression matrix.
(**B**) Phase portraits showing the ratio of unspliced and spliced RNA for more top-ranked genes driving the dynamic flow from cluster C4 to C6, along with their expression and velocity level within the three tumor clusters.
(**C**) Gene expression dynamics resolved along the pseudotime direction showing a clear cascade of transcription of the top-ranked genes.
(**D**) Read coverage mapped to the reference genome location for the selected small RNAs.

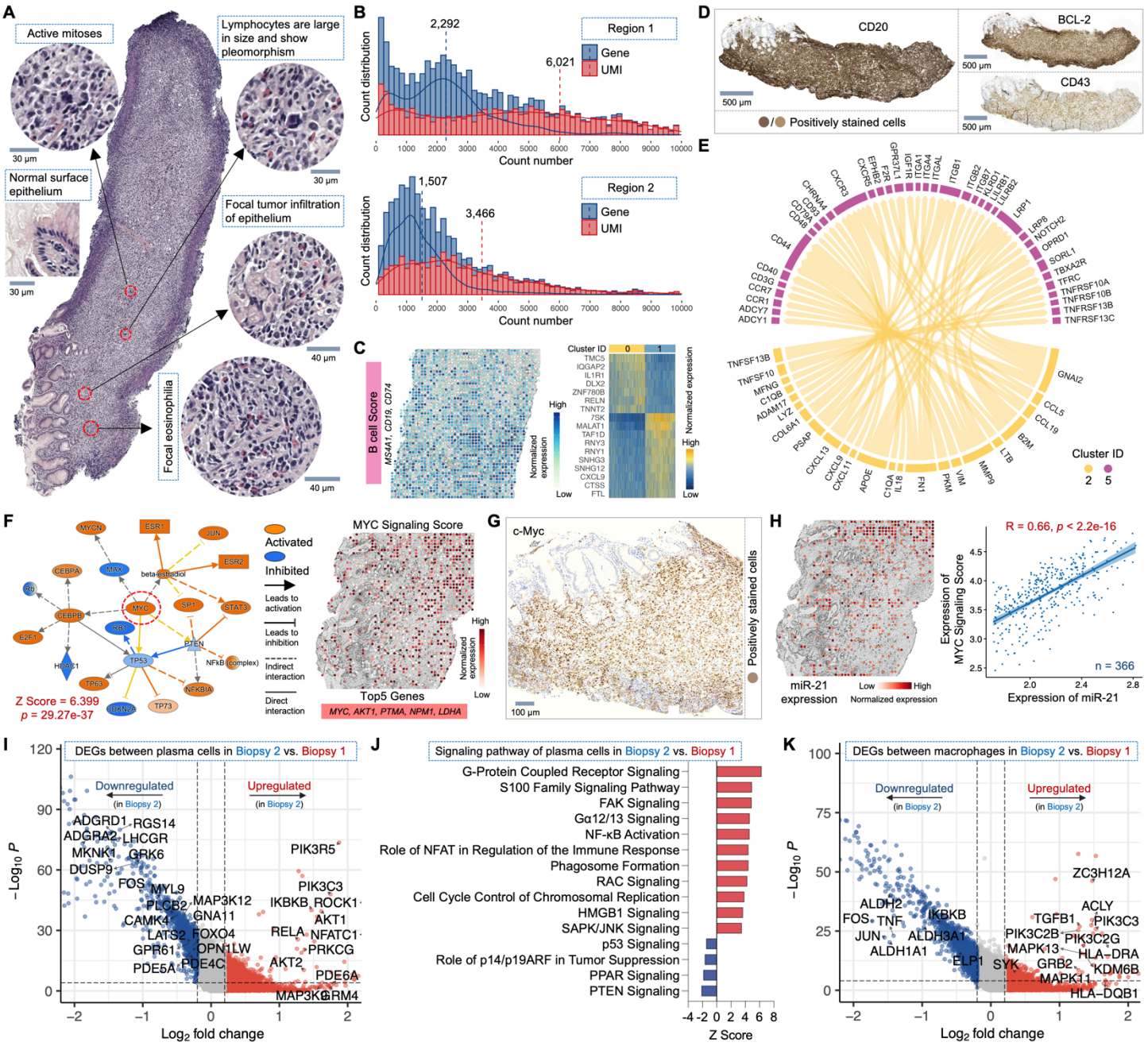

Figure S7. Spatial transcriptome and microRNA analysis of the DLBCL section

(**A**) H&E staining of an adjacent section with key histological information annotated by a pathologist.
(**B**) Distribution of detected gene/UMI counts per spatial pixel within two DLBCL regions. Only reads mapped to the exonic region were considered. Dashed lines represent the average gene or UMI count level.
(**C**) Left: Spatial expression of the B cell Score in the Region 1 section. Genes defining this module score are listed. Right: heatmap showing top ranked DEGs defining each cluster identified in the Region 1 section.
(**D**) IHC staining of CD20 and canonical markers commonly detected in DLBCL tumor cells (BCL-2 and CD43) on adjacent sections.

(**E**) Ligand-receptor interactions between tumor B cell clusters 2 and 5. Edge thickness is proportional to correlation weights.
(**F**) Left: mechanistic network analysis identifying a significant activation of the master regulator MYC in tumor B cells. Right: spatial expression of the MYC Signaling Score. Top 5 genes defining this module score are listed.
(**G**) IHC staining for c-Myc on an adjacent section.
(**H**) Left: spatial expression map of miR-21. Right: correlation analysis between miR-21 expression and the MYC Signaling Score. The Pearson correlation was calculated across 366 spatial pixels within the tumor region.
(**I**) Volcano plot showing DEGs between plasma cells in DLBCL vs. MALT biopsy.
(**J**) Signaling pathways regulated by DEGs identified in (I).
(**K**) Volcano plot showing DEGs between macrophages in DLBCL vs. MALT biopsy.
In (F), and (J), z score is computed and used to reflect the predicted activation level (z>0, activated; z<0, inhibited; z≥2 or z≤−2 can be considered significant).